Journal of Alloys and Compounds 753 (2018) 11–17

Contents lists available at ScienceDirect

Journal of Alloys and Compounds

journal homepage: http://www.elsevier.com/locate/jalcom

Fabrication and mechanical properties of high purity of Cr_2AlC coatings by adjustable Al contents

Jingzhou Liu [a, b], Xiao Zuo [b], Zhenyu Wang [b], Li Wang [b], Xiaochun Wu [a], Peiling Ke [b, *], Aiying Wang [b, **]

[a] School of Materials Science and Engineering, Shanghai University, Shanghai 200072, China
[b] Key Laboratory of Marine Materials and Related Technologies, Zhejiang Key Laboratory of Marine Materials and Protective Technologies, Ningbo Institute of Materials Technology and Engineering, Chinese Academy of Sciences, Ningbo 315201, China

ARTICLE INFO

Article history:
Received 4 January 2018
Received in revised form
3 April 2018
Accepted 8 April 2018
Available online 19 April 2018

Keywords:
Cr-Al-C coating
Al content
MAX phase
Phase structure
Mechanical property

ABSTRACT

The effect of Al content on phase structure and mechanical properties of vacuum annealed Cr-Al-C coatings was investigated. Cr-Al-C coatings were deposited by co-sputtering of Cr_2Al and Al targets in optimized CH_4/Ar atmosphere. The atomic content of Al was adjusted through the control of Al target current from 0.5 A to 3.0 A, thus Cr-Al-C coatings with different stoichiometric ratios were obtained. After 1.5 h thermal annealing at 750 °C in vacuum, Cr_2AlC MAX phase was observed from the XRD measurements. The Rietveld refinement of XRD spectra results indicated that the annealed coatings were composed of Cr_2AlC, Al_8Cr_5 and Cr_7C_3 phases with different amounts. With the increase of Al content, the hardness and modulus of the Cr_2AlC MAX phase coatings varied from 10.17 to 19.00 GPa and 198.43 to 267.62 GPa, respectively, while the toughness suffered an obvious decline. HRTEM analysis demonstrated that the excess of Al content resulted in the formation of Al_8Cr_5 and Al segregation at grain boundaries, which led to the deterioration of mechanical properties.

1. Introduction

MAX phases are ternary nanolayered metal carbides or nitrides with the general formula $M_{n+1}AX_n$, where M refers to early transition metal, A on behalf of IIIA or IVA elements, X represents C or N, n = 1, 2 or 3. The crystal structures of metallic (M-A) and covalent/ionic (M-X) bonding nature enable them to combine the properties of both metals and ceramics [1,2] such as high strength, outstanding oxidation resistance, good thermal shock resistance and damage tolerance, *etc* [3–6]. Benefiting from the formation of a protective Al_2O_3 layer well adhered to the surface, Cr_2AlC MAX phase attracts many attentions for the potential applications in high temperature oxidation and hot corrosion resistance [5,7–9]. Meanwhile, it exhibits excellent mechanical properties, including relative high hardness and Young's modulus, intermediate fracture toughness, good flexural strength, compression strength [10,11], electrical and thermal conductors [12]. Various methods have been applied to fabricate Cr_2AlC MAX phase coatings in recent years, including pulsed electro spark deposition [13], cathodic arc deposition [14], pulsed laser deposition [15], plasma spraying [16] and magnetron sputtering. Particularly, direct current magnetron sputtering (DCMS) takes the advantages of depositing dense and uniform coatings. Therefore, it is widely utilized to synthesize MAX phase coatings.

It has been reported that the purity of MAX phase in the coatings is the pre-requisite for achieving the excellent performances [17]. Usually, the fabricated MAX phase coatings contain a certain amount of impurities, such as binary carbides/nitrides and intermetallic compounds. In magnetron sputtering processes, composition deviation between coatings and targets will lead to the non-stoichiometric coatings, where impurity phases exist. Stanislav et al. [18] reported that the sputtering yields and transport efficiency of sputtered species were distinct for different target elements, which led to composition deviation between the deposited Cr-Al-C coatings and the Cr_2AlC compound targets. These differences always presented as the loss of C and Al in deposited coatings. Meanwhile, it has been reported that a certain excess Al in the as-deposited coating is benefit for the formation of Cr_2AlC MAX phase in the following post-heat treatment process [19–21]. For the

* Corresponding author.
** Corresponding author.
E-mail address: kepl@nimte.ac.cn (P. Ke).

https://doi.org/10.1016/j.jallcom.2018.04.100
0925-8388/

purpose of synthesizing dense and high-purity Cr_2AlC MAX phase coatings, we applied an additional Al target to adjust Al contents of the coatings, which co-sputtered with Cr_2Al target in optimized CH_4/Ar atmosphere. Then a process of post-heat treatment at 750 °C in vacuum environment was followed. The aim of this work is to investigate phase compositions and mechanical properties of Cr-Al-C coatings with different Al contents after annealing processes. The phase compositions are analyzed by Rietveld refinement method from the XRD spectra. The structural and mechanical properties are also characterized by SEM, TEM, XRD and nanoindentation. The relationship between phase composition and mechanical properties is discussed in terms of microstructure evolution in the coatings.

2. Experimental setup

2.1. Sample fabrication

Cr-Al-C coatings with different Al contents were deposited on Ti-6Al-4V (TC4) substrates by a DC magnetron sputtering system, where the hybrid CH_4/Ar mixture was used as the precursor gas with an optimized flow ratio of CH_4:Ar = 1:4. The size of TC4 substrates which were polished to 3000-grit (Ra≤22 nm) by SiC paper was 15 mm × 10 mm × 2 mm. The nominal composition of TC4 is list in Table 1. A stoichiometric Cr_2Al compound target (produced by powder metallurgical process) and an additional Al target with the purity of 99.9% were co-sputtered to adjust the Al content in the coatings. The size of both targets was 400 mm × 100 mm × 7 mm. Before the deposition process, TC4 substrates were ultrasonically cleaned in acetone for 15 min, and quickly dried in warm air. Then they were fixed on a rotational substrate holder in front of Cr_2Al target with a distance of about 12 cm. A schematic diagram of the deposition experiment arrangement is shown in Fig. 1. When the base pressure of the vacuum chamber was around 2.6×10^{-3} Pa, the chamber was filled with Ar gas to reach a pressure of 1.1 Pa, which was followed the glow discharge process with −300 V pulsed DC bias (100 kHz, duty cycle: 90%) on the substrates for 40 min to remove the surface contaminations and achieve better coating adhesion.

During the deposition process, the current applied on Cr_2Al target was fixed at 2.5 A, while the current on Al target was varied from 0.5 to 3.0 A, in order to tailor the Al content in the coatings. The working pressure was kept at 0.48 Pa by controlling the main valve of the vacuum chamber. The substrate bias was set at −200 V, no intentional heating of the substrates was conducted. The detailed deposition parameters of the Cr-Al-C coatings are listed in Table 2. After deposition, a vacuum annealing process was conducted at 1.0×10^{-2} Pa for the deposited coatings to obtain Cr_2AlC MAX phase. The heating rate was about 5 °C/min. After 1.5 h thermal insulation at 750 °C, the samples were cooled inside the furnace to room temperature.

2.2. Characterization methods

The crystal structures of the deposited and annealed coatings were characterized by X-ray diffraction (XRD), using a BrukerD8 Advance diffractometer with Cu Kα radiation, operating in θ-θ configurations and collecting data over a 2θ-range from 10° to 90°.

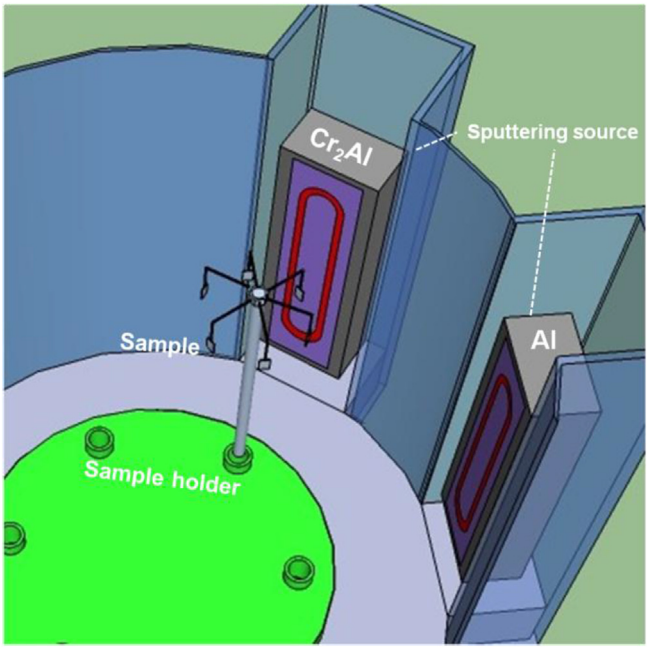

Fig. 1. Schematic diagram of the experiment arrangement.

Table 2
Deposition parameters for Cr-Al-C coatings.

Parameters	Values
Al target current (A)	0.5, 1.0, 2.0, 3.0
Cr_2Al target current (A)	2.5
Flow rates of CH_4/Ar (sccm)	20/80
Pressure (Pa)	0.48
Substrate bias voltage (V)	−200
Target to substrate distance (cm)	12

In order to quantitatively analyze the phase compositions of annealed Cr-Al-C coatings with different Al contents, all XRD patterns were processed using the Bruker TOPAS software to do Rietveld refinement. For the refinement procedure, the crystal structure files (.cif) and XRD patterns with different Al content were used. The emission profile (.lam) was represented by CuKα5.lam and the atomic positions of C (0, 0, 0), Cr (1/3, 2/3, 0.086), Al (2/3, 1/3, 0.25) in the unit cell were used in the Rietveld refinement [22]. The global parameters, such as zero error, air scattering factor and phase scale factors were refined in the initial refinement cycles. The background was fitted by using a Chebyshev function with 5 terms of the polynomial equation. The refinement was carried out for several cycles until a stable weighted reliability factors (Rwp) and satisfactory fits were obtained.

The chemical compositions were examined by scanning electron microscope (SEM, FEI Quanta FEG 250) equipped with an energy-dispersive X-ray spectrometry (EDS) using an EDAX Sapphire Si (Li) detector. The microstructure of the coatings were characterized using SEM and transmission electron microscope (TEM, Tecnai F20, US). TEM cross-sectional view images were obtained by a focused ion beam (FIB) process (Auriga, Germany), and a

Table 1
The element contents of TC4 substrate.

Element	Al	V	Fe	C	N	O	H	Ti
wt%	5.61	3.72	0.151	0.031	0.017	0.16	0.001	balance

layer of Pt was deposited to protect the surface layer from the damage of ion bombardment. Mechanical properties were measured by a MTS-G200 nanoindenter tool in a continuous stiffness measurement mode with a Berkovich diamond tip and maximum indentation depth of 2000 nm. All samples were mirror polished before surface nanoindentation measurements. The roughness of the substrate and deposited coatings were measured by surface profilometer (Alpha-step IQ, USA), and the Ra of all deposited coatings were less than 24 nm. The thickness of all deposited coatings is about 6 μm. The characteristic hardness of the coating was chosen in the depth of 500 nm where the hardness with indentation depth was stable and not affected by the substrate. Six replicate indentations were conducted for each coating to evaluate the average hardness (H) and Young's modulus (E) from load–displacement curves using the Oliver and Pharr method [23]. Vickers indentation tests were performed on a MVS-1000D1 Automatic digital micro hardness tester with the normal load of 0.98 N to test the toughness of the coating.

3. Results and discussions

3.1. Microstructure and phase composition of Cr-Al-C coatings with various Al contents

EDS results (Fig. 2(a)) indicated that with the increase of Al target current from 0.5 to 3.0 A, the Al content in the annealed coatings significantly increased from 23.67 to 42.74 at%. The decreases of Cr and C content in the annealed coatings were observed along with the increase of Al content. The ratio of Cr/Al decreased from 2.81 to 1.16 as shown in Fig. 2(b). There was no obvious change in the content of Al after thermal annealing in vacuum.

Fig. 3 shows the XRD patterns of as-deposited and annealed coatings. With increase of the Al target current from 0.5 A to 3 A, all the as-deposited Cr–Al–C coatings possessed an amorphous structure, according to 2θ around 42° as shown in Fig. 3(a). This might be the reason that the energy of adsorbates in sputtering deposition processes of Cr-Al-C coatings is too low to form MAX phase at room temperature [24]. Abdulkadhim et al. [25] studied the crystallization kinetics of amorphous Cr_2AlC coating through differential scanning calorimetry (DSC) and XRD. They found that the transformation temperature of Cr_2AlC MAX was 610 °C and the transformation was controlled by diffusion. In order to promote the diffusion process, all deposited coatings were annealed at 750 °C in vacuum for 1.5 h to improve crystallization. As shown in Fig. 3(b), all the annealed coatings showed the crystalline peaks in XRD patterns, indicating the enhanced well crystallization characteristics. However, through the Cr-Al-C phase diagram, we can concluded that other intermediate phases such as $AlCr_2$, Cr_7C_3, Cr_3C_2, and Al_8Cr_5 would coexist with Cr_2AlC MAX phase when the stoichiometric ratio of Cr:Al:C deviates from 2:1:1 at 750 °C [26,27]. Therefore, it is necessary to perform refinement analysis. Finally, it was certain that Cr_2AlC, Cr_7C_3 and Al_8Cr_5 phases matched the XRD patterns, no $AlCr_2$ and Cr_3C_2 phases existed in the coatings. The different intensities of peaks in the XRD patterns for the annealed Cr-Al-C coatings implied that the Al_8Cr_5 phase crystallization was strongly dependent upon the Al content in the coatings. As mentioned above, the transformation of Cr_2AlC MAX was controlled by diffusion. At 750 °C, the liquid Al (melting point is 660 °C) will promote the diffusion process. Meanwhile, we can conclude from the Cr-Al-C phase diagram that with the increase of Al content, the excess Al in the coating inclined to form Al_8Cr_5 which exhibit a higher and higher peak in the low angle diffraction region [27].

Fig. 4 shows the final Rietveld plot, where the blue line demonstrates experimental data, the red line denotes calculated intensities, and the grey line in the bottom represents the difference between measured intensities and calculated intensities. The Rwp of the refinements shown in Table 3 were all less than 8, indicating that the fitting results were credible. Through Rietveld refinement analysis, it was found that all the annealed coatings were composed of Cr_2AlC, Al_8Cr_5 and Cr_7C_3 with different weight percentages. The detailed structure information is listed in Table 3. The lattice parameter (*a*) derived from the Rietveld refinement varied from 2.85 to 2.86, while lattice parameter (*c*) changed from 12.94 to 12.85, both of these two parameters were in accordance with the results reported [22].

Fig. 5 shows the variation of Cr_2AlC MAX phase content and Cr/Al ratio in the annealed Cr-Al-C coatings with different Al target currents. With the increase of Al target current, Cr/Al ratio decreased from 2.81 to 1.16, the MAX phase content increased first and then decreased, a maximum value of 86.62 wt% was obtained when the ratio of Cr/Al was 2.09 (Al target current at 1.0 A). The content of Al_8Cr_5 and Cr_7C_3 was 6.31 and 7.07 wt%, respectively. The content of MAX phase would be higher after long time annealing because of the more sufficient diffusion process. However, the grain would grow coarser after overlong annealing [24], which did harm to the mechanical properties of the coatings. When the Cr/Al ratio exceeded 2.09, the content of Al_8Cr_5 significantly increased with the improvement of Al content, and reached 28.28 wt% when Cr/Al was 1.16 (Al target current at 3.0 A). On the contrary, the content of Cr_7C_3 showed an obvious decline trend. Therefore, it could be concluded that the higher peak intensity at 13.8° was due to the

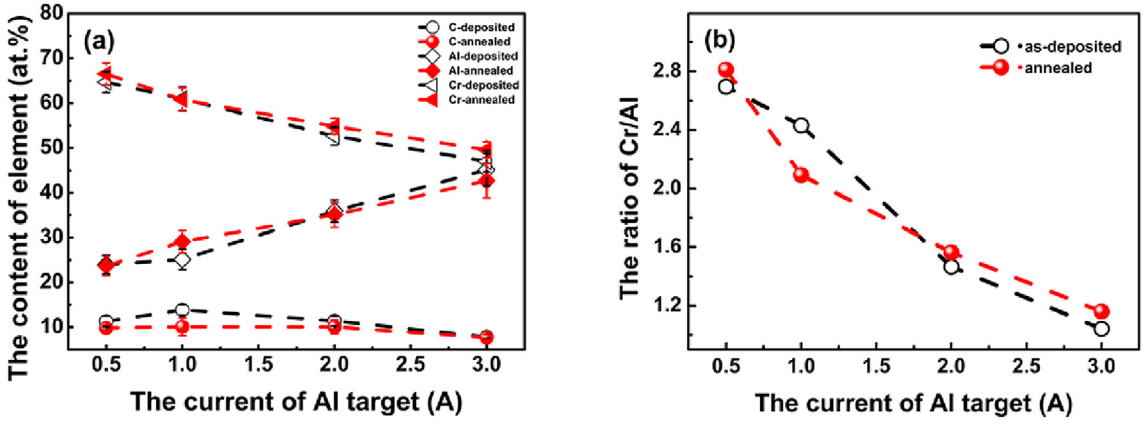

Fig. 2. (a) Element contents and (b) Cr/Al ratios in as-deposited and annealed coatings synthesized at different Al target currents.

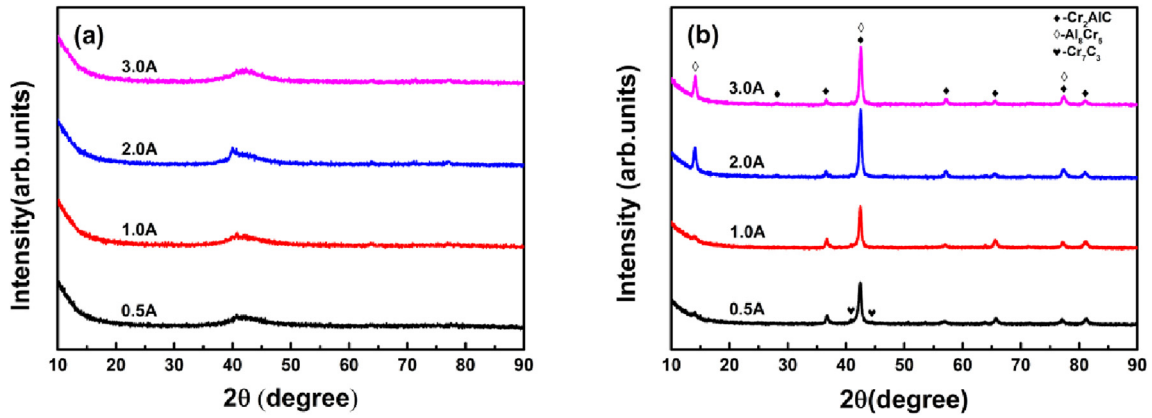

Fig. 3. XRD patterns of the (a) as-deposited and (b) annealed coatings.

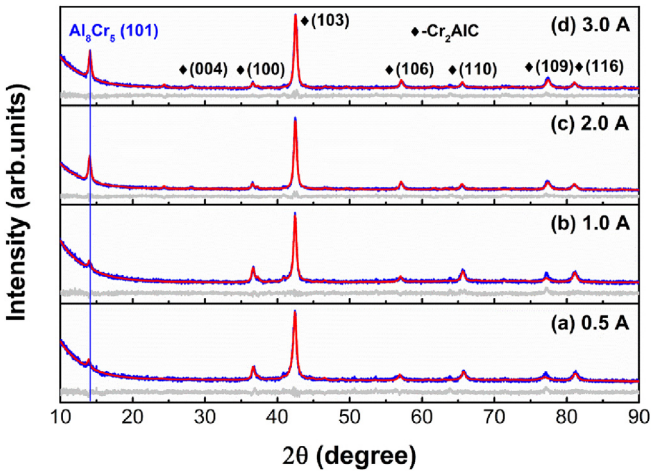

Fig. 4. Rietveld refinement for annealed coatings deposited at (a) 0.5 A (b) 1.0 A (c) 2.0 A (d) 3.0 A.

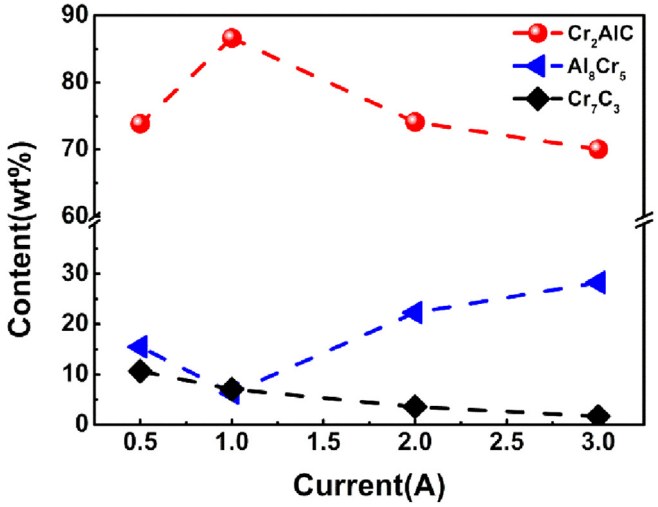

Fig. 5. The contents of Cr_2AlC MAX phase, Al_8Cr_5 and Cr_7C_3 with various Al target currents.

accumulation of Al_8Cr_5 (110) peak rather than the increase of Cr_2AlC (002).

To further identify the microstructure of the annealed Cr-Al-C coatings with different Al contents, the annealed coatings deposited with Al target currents at 1.0 A and 3.0 A were selected to conduct TEM cross-section analysis representatively. As shown in Fig. 6(a) and (e), a columnar microstructure along the growth direction of the Cr-Al-C coatings were all observed in the bright field TEM image at a low magnification. However, noted that the coatings were dense and free of cracks. Fig. 6(b) shows the selected area electron diffraction (SAED) pattern of Al current at 1.0 A. The phase compositions of Cr_2AlC, Al_8Cr_5 and Cr_7C_3. Cr_2AlC with the diffraction information of the plane (100), (103), (106), (110), (109), (116) was identified, which was consistent with the Rietveld results. In addition, the diffraction plane of Al_8Cr_5 (101) was discerned in coatings deposited with Al target current at 3.0 A, as shown in Fig. 6(e), which agreed well with the XRD results. In general, Cr_2AlC has a hexagonal structure with space group *P*63/*mmc*. The stacking sequence of the Cr_2AlC along the [0001] direction is alternatively stacked by one Al layer and two Cr layers. This stacking sequence can be clearly seen in the high resolution TEM image (HRTEM), illustrated in Fig. 6(c, d, e), with the electron beam paralleling to the $[11\bar{2}0]$ direction. Moreover, the lattice parameter *c* derived from the HRTEM was 1.29 nm, which was in good accordance with the Rietveld refinement results.

In comparison with TEM bright-field image, the scanning transmission electron microscope (STEM) technique enables to reveal atomic number (Z) contrast, which directly indicates the distribution of various elements. Therefore, STEM was carried out to demonstrate the distribution of Cr and Al element in micro-regions. As shown in Fig. 7, the differences in contrast represented

Table 3
The Rietveld refinement results of coatings with different Al contents.

Current (A)	Cr/Al	Cr_2AlC (wt%)	a (Å)	c (Å)	Al_8Cr_5 (wt%)	Cr_7C_3 (wt%)	Rwp
0.5	2.81	73.85	2.85	12.935	15.5	10.66	6.992
1.0	2.09	86.62	2.855	12.899	6.31	7.07	7.051
2.0	1.56	74.11	2.86	12.86	22.31	3.58	7.887
3.0	1.16	70.04	2.865	12.853	28.28	1.68	7.414

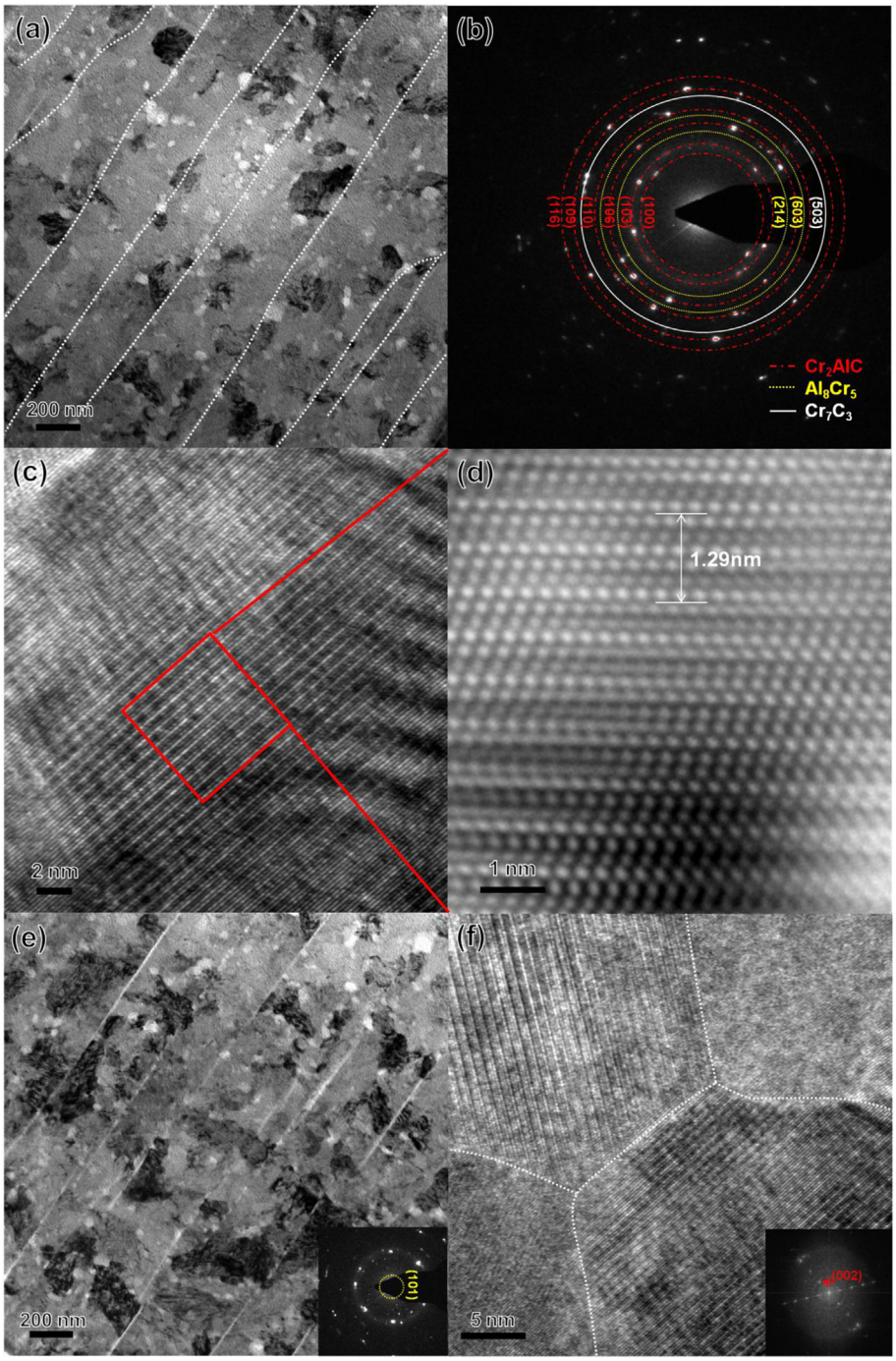

Fig. 6. TEM cross-sectional images of the annealed coatings: (a) Bright-field image, (b) the corresponding SAED pattern and (c, d) HRTEM image of Al current at 1.0 A; (e) Bright-field image and SAED pattern and (f) HRTEM image and FFT of Al current at 3.0 A.

different phases in STEM image, the EDS mapping results in the red rectangular region displayed an obvious Al enrichment in the dark grey region. Combined with the XRD results, the dark grey region should be composed of Al_8Cr_5 intermetallics while the dark grey color at columnar grain boundary was assigned to Al segregation.

3.2. The mechanical properties of annealed Cr-Al-C coatings with different Al contents

Fig. 8 shows the hardness (H) and elastic modulus (E) of annealed Cr-Al-C coatings with different Al contents. Hardness indicates the resistance when indenter is pressed during plastic deformation, while a high modulus (E) represents the distribution of given load on a larger area [28]. When the Al target current increased from 0.5 A to 3.0 A, the hardness of the coatings was changed in a range from 10.61 to 19.00 GPa. In particular, the maximum hardness of 19.00 GPa was found at the 1.0 A Al target current, which corresponded to a Cr/Al atomic percentage ratio of 2.09 and Cr_2AlC MAX phase purity of 86.62%.

Considering Leyland et al. found that elastic strain to failure (H/E) played an important role in wear control [29], and Johnson et al. [30] reported that the ratio of plastic strain to failure (H^3/E^2)

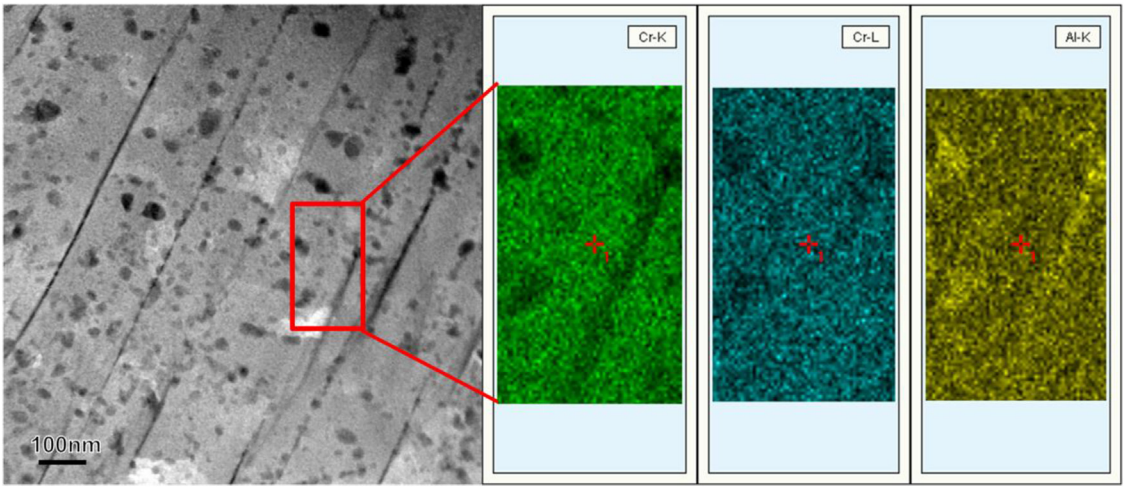

Fig. 7. STEM image of 1.0 A and corresponding EDS mapping of the red rectangular region. (For interpretation of the references to color in this figure legend, the reader is referred to the Web version of this article.)

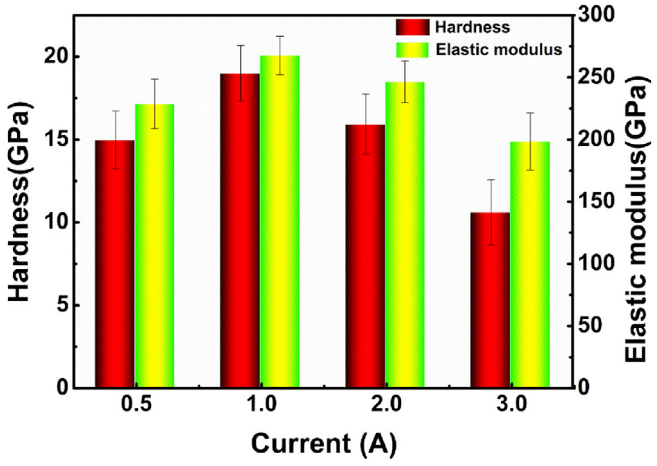

Fig. 8. The hardness and elastic modulus of annealed Cr-Al-C coatings with different Al contents.

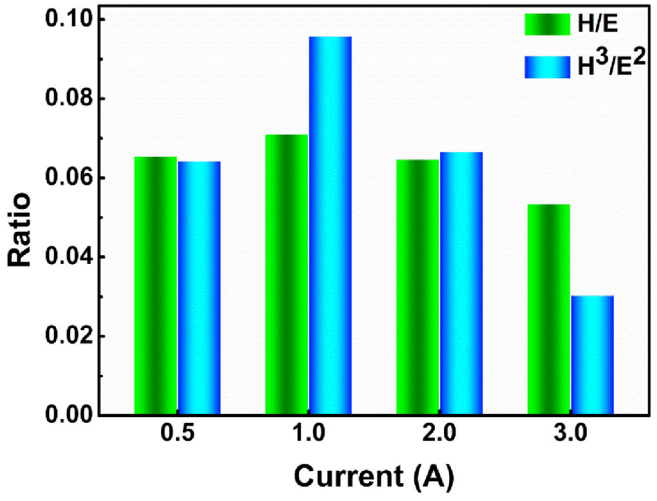

Fig. 9. The H/E and H^3/E^2 of annealed Cr-Al-C coatings with different Al contents.

indicates coatings resistance of plastic deformation, calculated the H/E and H^3/E^2 for the deposited coatings. When the Al current was changed from 0.5 A to 3.0 A, as shown in Fig. 9, the value of H/E changed slightly from 0.065 to 0.053, and the maximum value of 0.071 was obtained at 1.0 A Al target current, indicating the best wear resistance among the four coatings. The variation of H^3/E^2 showed similar trend as H/E, which also reached the maximum at 1.0 A Al target current, representing a better toughness than other three coatings. When the ratio of Cr/Al in the coating exceeded 2:1, the excess Al in the coating tended to form ductile intermetallic Al_8Cr_5, leading to the reduced hardness finally. At the same time, the segregation of Al at grain boundary could suppress the dislocation movement, which brought about the deterioration in the toughness of annealed coatings.

In order to gain insight to the toughness of deposited coatings, Vickers indentations were conducted. Fig. 10 shows the corresponding crack patterns. The coatings deposited at 0.5 A and 1.0 A displayed excellent toughness, as no crack along radial direction and axial direction was detected after the tests. However, further increasing the Al content to 2.0 A, two radial microcracks emerged in the coating surface, indicating the degradation of the toughness. The radial crack became much more serious in the coatings deposited at 3.0 A Al target current, which implied the increase of brittleness. This toughness evolution could be in accordance with the H^3/E^2 results. As mentioned above, the decline of mechanical properties were mainly due to the increasing number of ductile intermetallic Al_8Cr_5 as well as Al segregation at the grain boundary. In this case, the coatings deposited at 1.0 A Al target current, representing the Al content at 29.07 at% and Cr/Al ratio at 2.09, owed the combined superior mechanical properties due to the tailored dense MAX phase structure.

4. Conclusions

By using a DC magnetron sputtering system, Cr-Al-C coatings with different atomic contents of Al were synthesized through adjusting the current of an additional Al target from 0.5 A to 3.0 A. Annealed Cr-Al-C coatings with Cr:Al = 2.09:1 were obtained when Al target current was 1.0 A. It was found that all the annealed coatings were composed of Cr_2AlC, Al_8Cr_5 and Cr_7C_3. The content of Al_8Cr_5 varied from 6.31 wt% to 28.28 wt%, while the Cr_7C_3 content in coating observed an obvious decline (from 10.66 wt% to 1.68 wt %) along with the increase of Al content. The deterioration of

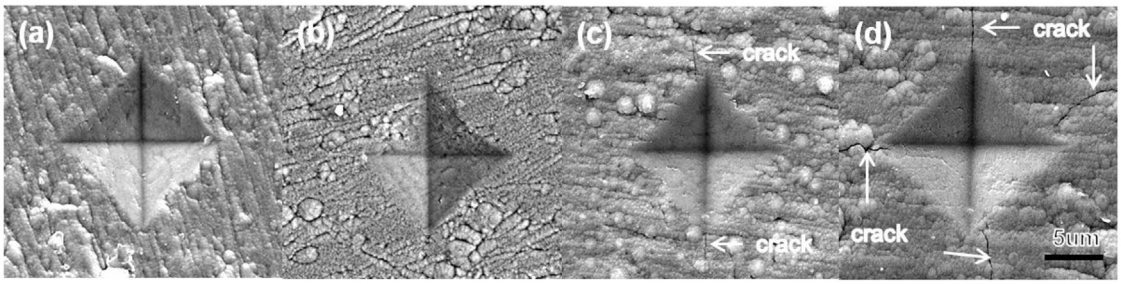

Fig. 10. Vickers indentation morphology of the annealed Cr_2AlC coating with different Al target current (a) 0.5 A, (b) 1.0 A, (c) 2.0 A, (d) 3.0 A.

mechanical properties was mainly due to the formation of ductile intermetallic Al_8Cr_5 and Al segregation at grain boundary. The most important result was that the maximum purity of Cr_2AlC MAX phase with 86.62 wt% and good mechanical properties were obtained for the near-stoichiometric annealed Cr-Al-C coatings. In particular, the Cr_2AlC MAX coatings had a maximum hardness and elastic modulus of 19.00 GPa and 267.62 GPa, respectively. The value of H/E, H^3/E^2 and vickers indentations patterns implied a quite good toughness and wear resistance, which benefited the potential application for the mechanical components in abrasive wear conditions.

Acknowledgements

This work was supported by the National Natural Science Foundation of China (51522106 and 51611130061), the National Science and Technology Major Project of China (2015ZX06004-001), and Zhejiang Key Research and Development Program (2017C01001). We authors sincerely thank Prof. Magnus Odén at Linköping University for helpful discussion.

References

[1] M.W. Barsoum, The $M_{N+1}AX_N$ phases A new class of solids: thermodynamically stable nanolaminates, Prog. Solid State Chem. 28 (2000) 201–281.
[2] P. Eklund, M. Beckers, U. Jansson, H. Högberg, L. Hultman, The $M_{n+1}AX_n$ phases: materials science and thin-film processing, Thin Solid Films 518 (2010) 1851–1878.
[3] M. Barsoum, T. El-Raghy, The MAX phases: unique new carbide and nitride materials, Am. Sci. 89 (2001) 334.
[4] Y.C. Zhou, X.H. Wang, Deformation of polycrystalline Ti_2AlC under compression, Mater. Res. Innovat. 5 (2001) 87–93.
[5] Z.J. Lin, M.S. Li, J.Y. Wang, Y.C. Zhou, High-temperature oxidation and hot corrosion of Cr_2AlC, Acta Mater. 55 (2007) 6182–6191.
[6] W. Tian, Z. Sun, H. Hashimoto, Y. Du, Compressive deformation behavior of ternary compound Cr_2AlC, J. Mater. Sci. 44 (2008) 102–107.
[7] W. Tian, P. Wang, Y. Kan, G. Zhang, Oxidation behavior of Cr_2AlC ceramics at 1,100 and 1,250 °C, J. Mater. Sci. 43 (2008) 2785–2791.
[8] D.B. Lee, S.W. Park, Oxidation of Cr_2AlC between 900 and 1200 °C in air, Oxid. Met. 68 (2007) 211–222.
[9] S. Li, L. Xiao, G. Song, X. Wu, W.G. Sloof, S. van der Zwaag, Y. Zhou, Oxidation and crack healing behavior of a fine-grained Cr_2AlC ceramic, J. Am. Ceram. Soc. 96 (2013) 892–899.
[10] M.W. Barsoum, M. Radovic, Elastic and mechanical properties of the MAX phases, Annu. Rev. Mater. Res. 41 (2011) 195–227.
[11] W. Tian, Z. Sun, Y. Du, H. Hashimoto, Mechanical properties of pulse discharge sintered Cr_2AlC at 25–1000 °C, Mater. Lett. 63 (2009) 670–672.
[12] W. Tian, P. Wang, G. Zhang, Y. Kan, Y. Li, D. Yan, Synthesis and thermal and electrical properties of bulk Cr_2AlC, Scr. Mater. 54 (2006) 841–846.
[13] E.I. Zamulaeva, E.A. Levashov, T.A. Sviridova, N.V. Shvyndina, M.I. Petrzhik, Pulsed electrospark deposition of MAX phase Cr_2AlC based coatings on titanium alloy, Surf. Coating. Technol. 235 (2013) 454–460.
[14] J.J. Li, Y.H. Qian, D. Niu, M.M. Zhang, Z.M. Liu, M.S. Li, Phase formation and microstructure evolution of arc ion deposited Cr_2AlC coating after heat treatment, Appl. Surf. Sci. 263 (2012) 457–464.
[15] C. Lange, M.W. Barsoum, P. Schaaf, Towards the synthesis of MAX-phase functional coatings by pulsed laser deposition, Appl. Surf. Sci. 254 (2007) 1232–1235.
[16] Z. Zhang, S.H. Lim, J. Chai, D.M.Y. Lai, A.K.H. Cheong, K.L. Cheong, S.J. Wang, H. Jin, J.S. Pan, Plasma spray of Ti_2AlC MAX phase powders: effects of process parameters on coatings' properties, Surf. Coating. Technol. 325 (2017) 429–436.
[17] G. Ying, X. He, M. Li, W. Han, F. He, S. Du, Synthesis and mechanical properties of high-purity Cr_2AlC ceramic, Mater. Sci. Eng. A 528 (2011) 2635–2640.
[18] S. Mráz, J. Emmerlich, F. Weyand, J.M. Schneider, Angle-resolved evolution of the composition of Cr–Al–C thin films deposited by sputtering of a compound target, J. Phys. D Appl. Phys. 46 (2013), 135501.
[19] R. Mertens, Z. Sun, D. Music, J.M. Schneider, Effect of the composition on the structure of Cr-Al-C investigated by combinatorial thin film synthesis and ab initio calculations, Adv. Eng. Mater. 6 (2004) 903–907.
[20] C. Walter, D.P. Sigumonrong, T. El-Raghy, J.M. Schneider, Towards large area deposition of Cr_2AlC on steel, Thin Solid Films 515 (2006) 389–393.
[21] X. Duan, L. Shen, D. Jia, Y. Zhou, S. van der Zwaag, W.G. Sloof, Synthesis of high-purity, isotropic or textured Cr_2AlC bulk ceramics by spark plasma sintering of pressure-less sintered powders, J. Eur. Ceram. Soc. 35 (2015) 1393–1400.
[22] Q. Huang, H. Han, R. Liu, G. Lei, L. Yan, J. Zhou, Q. Huang, Saturation of ion irradiation effects in MAX phase Cr_2AlC, Acta Mater. 110 (2016) 1–7.
[23] W.C. Oliver, G.M. Pharr, An improved technique for determining hardness and elastic modulus using load and displacement sensing indentation experiments, J. Mater. Res. 7 (2011) 1564–1583.
[24] Y. Li, G. Zhao, Y. Qian, J. Xu, M. Li, Deposition of phase-pure Cr_2AlC coating by DC magnetron sputtering and post annealing using Cr-Al-C targets with controlled elemental composition but different phase compositions, J. Mater. Sci. Technol. 34 (3) (2017) 466–471.
[25] A. Abdulkadhim, M.t. Baben, T. Takahashi, V. Schnabel, M. Hans, C. Polzer, P. Polcik, J.M. Schneider, Crystallization kinetics of amorphous Cr_2AlC thin films, Surf. Coating. Technol. 206 (2011) 599–603.
[26] Z. Lin, Y. Zhou, M. Li, Synthesis, microstructure, and property of Cr_2AlC, J. Mater. Sci. Technol. 23 (2007) 721–746.
[27] J.C. Schuster, H. Nowotny, C. Vaccaro, The ternary systems: Cr-Al-C, V-Al-C, and Ti-Al-C and the behavior of H-Phases (M_2AlC), J. Solid State Chem. 32 (1980) 213–219.
[28] G.S. Kim, S.Y. Lee, J.H. Hahn, S.Y. Lee, Synthesis of CrN/AlN superlattice coatings using closed-field unbalanced magnetron sputtering process, Surf. Coating. Technol. 171 (2003) 91–95.
[29] A. Leyland, A. Matthews, On the significance of the H/E ratio in wear control: a nanocomposite coating approach to optimised tribological behaviour, Wear 246 (2000) 1–11.
[30] K.L. Johnson, Contact Mechanics, Cambridge University Press, 1985.